Spectral density functions of wind pressures on various low building roof geometries

K. Suresh Kumar[†]

Faculty of Building, Architecture and Planning, FAGO, Technical University of Eindhoven, Postbus 513, 5600 MB Eindhoven, The Netherlands

T. Stathopoulos[‡]

Centre for Building Studies, Concordia University, 1455 de Maisonneuve Blvd. W., Montreal, Quebec, H3G 1M8, Canada

Abstract. This paper describes in detail the features of an extensive study on Spectral Density Functions (SDF's) of wind pressures acting on several low building roof geometries carried out in a boundary layer wind tunnel. Various spectral characteristics of wind pressures on roofs with emphasis on derivation of suitable analytical representation of spectra and determination of characteristic spectral shapes are shown. Standard spectral shapes associated with various zones of each roof and their parameters are provided. The established spectral parameters can be used to generate synthetic spectra adequate for the simulation of wind pressure fluctuations on building surfaces in a generic fashion.

Key words: buildings; low-rise; roofs; spectral density function; wind pressures.

1. Introduction

Spectral density functions (SDF's) are utilized to describe how the energy associated with a time series is distributed in the frequency domain. The various characteristics of the time series such as level crossing rates and peak rates can also be determined using spectra. Most importantly, careful generation of SDF is necessary for the computer simulation of time series based on target SDF. For instance, wind pressure spectra are required for the digital simulation of pressure fluctuations on building surfaces based on the spectral representation method (Brockwell and Davis 1991, Suresh Kumar 1997). As compared to wind tunnel simulation, computer simulation is a feasible alternative to generate pressure time histories especially when several of them are required for extreme value analysis and fatigue design.

In the past, there have been several studies on quantifying wind velocity spectra, essential for the theoretical analysis of wind loads on buildings (Panofsky and McCormick 1954, Davenport 1961). Most recently, Tieleman (1995) presented unified spectral methods for the three-component velocity fluctuations in wind-tunnel generated shear flows and in the

---

† Post-doctoral Fellow, Formerly, Doctoral student at School for Building, Concordia University, Montreal, Canada
‡ Professor and Director

atmospheric boundary layer. On the other hand, wind pressure spectra have received only limited attention and isolated measurements have been carried out for specific cases in many studies. However, the classification of spectra of space-averaged pressures over flat roof panels (Stathopoulos et al. 1981) and the more recent attempt to describe basic shapes of spectra (Kasperski et al. 1996) are notable exceptions. In light of the unavailability of any systematic information on spectra of wind pressures acting on low building roofs, the present study was undertaken to establish overall spectral characteristics under various conditions with the help of wind tunnel measurements.

The paper discusses various characteristics of pressure spectra on low building roofs and suggests an empirical model for their description. Appropriate normalization has led to the classification of complex spectral patterns. Finally, the various zones of the roof and their corresponding spectral shapes in terms of their parameters are provided for various geometries. A few preliminary results of this study dealing primarily with flat roofs were reported in Suresh Kumar and Stathopoulos (1998a).

2. Theory

Some of the important properties of the SDF used in this investigation are briefly provided in this section. A fairly detailed analysis is provided by Vanmarcke (1983). For any zero-mean stationary random process, the spectral density function ($S(f)$) is defined as the Fourier transform of the autocorrelation function ($R(\tau)$) of the process, i.e.,

$$S(f) = \frac{2}{\pi} \int_0^\infty R(\tau) \cos(2\pi f \tau) d\tau \qquad (1)$$

where $S(f)$ is considered to be non-negative one-sided physical spectrum. The spectral moments, m_i, are defined by

$$m_i = \int_0^\infty f^i S(f) df, \qquad\qquad i = 0, 1, 2, \cdots \qquad (2)$$

in which m_0 represents the variance (σ^2) which is the area under $S(f)$. The spectral moments can be used to establish level crossing rates as well as peak rates of a narrowband stationary Gaussian random process. The zero up-crossing or down-crossing rate (N_0) of the process can be estimated by

$$N_0 = [m_2/m_0]^{1/2} \qquad (3)$$

whilst, the positive or negative peak rate (N_p) can be estimated by

$$N_p = [m_4/m_2]^{1/2} \qquad (4)$$

Since Eqs. (3) and (4) have been developed based on narrowband assumption, they must be used with caution in case of a broadband process. The broadband nature of a stationary random process can be quantified by using irregularity factor (ε) or bandwidth parameter (β). The irregularity factor (ε), a measure of distance to narrowband, can be evaluated by

$$\varepsilon = N_0/N_p \qquad (5)$$

The bandwidth parameter (β), a measure of the dispersion of the SDF around its central

frequency, can be estimated by

$$\beta = \sqrt{1 - \varepsilon^2} \tag{6}$$

The irregularity factor as well as bandwidth parameter range between 0 and 1. While $\varepsilon = 1$ and $\beta = 0$ represent a pure narrowband process, $\varepsilon = 0$ and $\beta = 1$ represent a pure broadband process. For more precise definition of terms and more details, see Vanmarcke (1983).

The form of the spectrum adopted in this study is the normalized SDF ($S(f)/\sigma^2$). The integral of the spectrum is

$$\int_0^\infty \frac{S(f)}{\sigma^2} \, df = 1 \tag{7}$$

Spectra are usually shown as a function of the reduced frequency, $F = fh/V$, where h is a typical building dimension, say mean roof height of the building, and V is the mean velocity at mean roof height. Spectra are conveniently drawn in logarithmic scales to show the energy that is spread over a wide range of frequencies.

3. Experimental procedure

The experiments were carried out in the boundary-layer wind tunnel of the Centre for Building Studies (CBS) of Concordia University, Montreal, Canada. The working section of the tunnel is 12.2 m long, 1.8 m wide and about 1.8 m high. Open-country as well as suburban terrain exposures were simulated in the tests. Mean velocity and turbulence intensity profiles are shown in Fig. 1. The boundary layer geometric scale is approximately 1:400. The wind speed at gradient height was approximately 11 m/s.

Plexiglass models of flat-roof, monoslope roof, and gable-roof buildings were tested for several wind angles. The dimensions of the models used in this study are reported in Table 1.
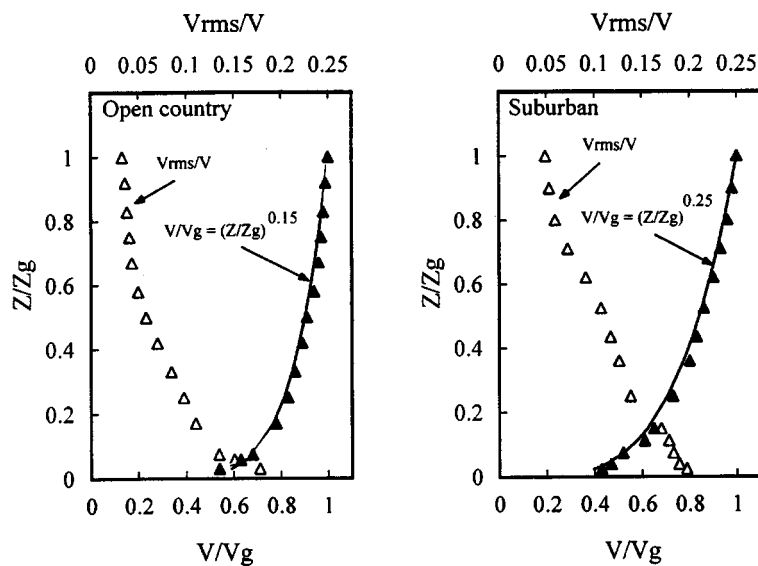

Fig. 1 Mean speed and turbulence intensity profiles for both terrains considered

Table 1 Models used in this study

	Dimensions		
	1	*b*	h_1
Monoslope Roof ($\alpha \approx 15°$)			
Full-Scale (m)	60.8	19.2	12.0
Model (mm)	152.0	48.0	30.0
Flat Roof			
Full-Scale (m)	43.2	43.2	15.0
Model (mm)	108.0	108.0	37.5
Gable Roofs ($\alpha \approx 19°$ and $\alpha \approx 45°$)			
Full-Scale (m)	60.8	39.2	12.0
Model (mm)	152.0	98.0	30.0

Note : 1 = length, b = width, h_1 = lower eave height, α = roof angle

In the first phase of this study, a number of roof tappings (Fig. 2a) were used not to determine detailed aerodynamic behaviour but to examine variability in pressure spectra and possible elimination of taps from future tests. In the second phase, tests were conducted only for the selected taps (Fig. 2b) from the first phase.

Pressure fluctuations were measured with SETRA 237 pressure transducers using a Scanivalve. The Scanivalve was connected to pressure tappings with plastic tubes 610 mm long with inside diameter of 1.6 mm. Restrictors were placed in the tubes to provide a flat frequency response up to 100 Hz. Frequencies of pressure fluctuations at most tappings are expected to be well below this value.

Pressure data were acquired in blocks of 8192 samples each at a sampling rate of 500 Hz using a waveform analyzer (DATA-6000) after each signal passed through a low-pass filter with a cut-off at a Nyquist frequency of 250 Hz. At a length ratio of 1:400 and mean velocity ratio of about 1:3.5, the resulting time history of approximately 16 seconds providing statistically stable mean and variance is equivalent to 30 minutes in full-scale. At the end of each sampling period, the measured pressure signals were converted to pressure coefficient signals by dividing them by the reference dynamic pressure at building height. Simultaneously, the pressure coefficient spectrum ($S(f)$) was also evaluated with the help of the DATA 6000 analyzer. Smoothing of the spectra has been done by ensemble averaging for 16 records.

4. Experimental results

A typical sample of normalized spectra of pressure fluctuations and the corresponding longitudinal spectrum of incident wind at building height without the presence of the building are shown in Fig. 3. Note that pressure spectral energy is distributed over a wide frequency range. At low frequencies, amplitudes of the pressure spectrum, mainly related to the turbulence in incident flow, are somewhat lower than those of the velocity spectrum. At high frequencies, pressure spectral amplitudes are significantly higher than wind spectral amplitudes. This additional energy in pressure spectra is contributed by small-scale turbulence caused by the interaction of incident wind turbulence with the building. This is common among all taps on the roof. A typical comparison between the model and full-scale wind pressure spectra is
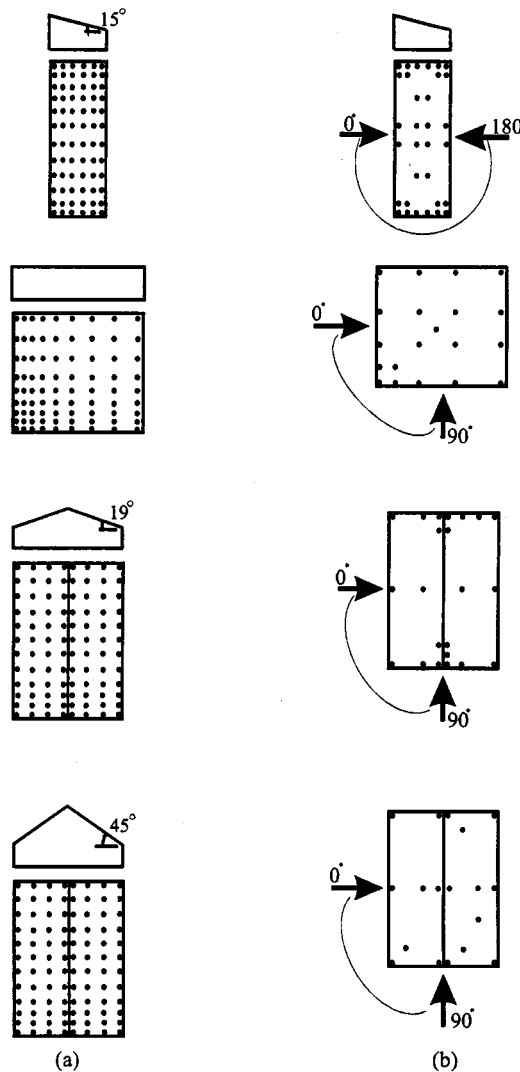
Fig. 2 Models and their corresponding tap locations used in the (a) first phase, and (b) second phase of the measurements

shown in Fig. 4. The full-scale spectra corresponds to tap 50101 of TTU building (Texas Tech ...... 1992). The full-scale time history was sampled at 40 Hz with a cut-off frequency at 10 Hz. At a length scale of 1:400 and a mean velocity ratio of about 1:3.5, the model sampling frequency and cut-off frequency were equivalent to about 4.3 Hz and 2.15 Hz in full scale. Note that the model and full-scale cases used for this comparison are slightly different in terms of building geometry and tap location. In particular, the model height was equivalent to about 15 m in full scale, while the full-scale building height was only 4 m. The comparison shows that the model spectrum is in reasonably good agreement with the full-scale. Some extraneous spikes caused by electrical noise do appear in the measured wind-tunnel spectra at harmonics of the electrical frequency. The significance of the spikes is estimated by measuring the area under the spikes, which is found to be within 5% of the corresponding variances in majority of
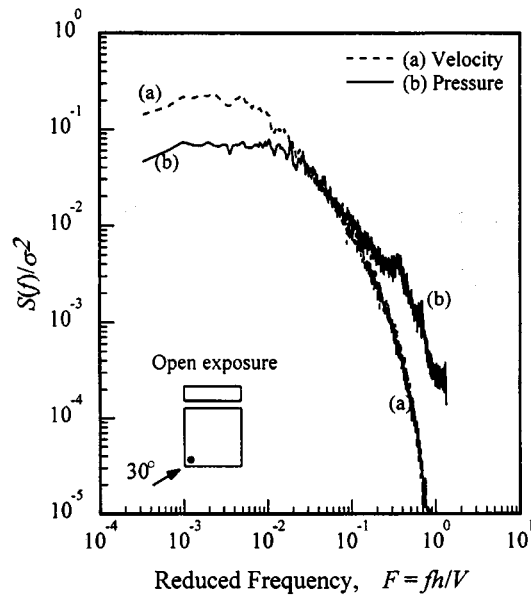
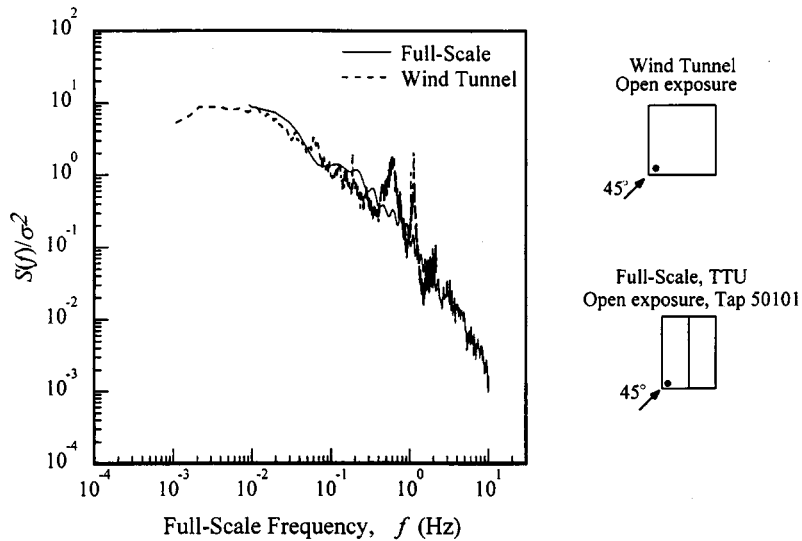Fig. 3 Sample spectra of wind velocity and wind pressure

Fig. 4 Comparison of wind pressure spectra

the cases.

Figs. 5 and 6 show typical samples of measured pressure spectra. A common feature found in all measurements is that, in general, the amplitude of the pressure spectrum decreases as the frequency increases. However, a small growth in spectral amplitudes at dimensionless frequencies (F) between 0.1 and 0.2 ($f \approx 20$ to 40 Hz) has been observed at taps located in the farwind (i.e., the windward edge region away from the windward corner in case of oblique wind angle) as well as leeward regions of the roof. These humps on the spectra are possibly associated with shedding of dominant eddies in those regions and can be observed for
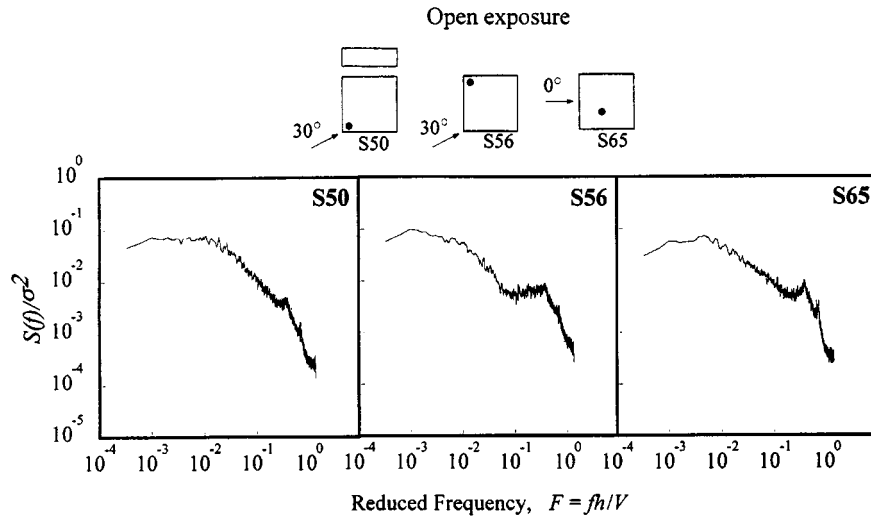
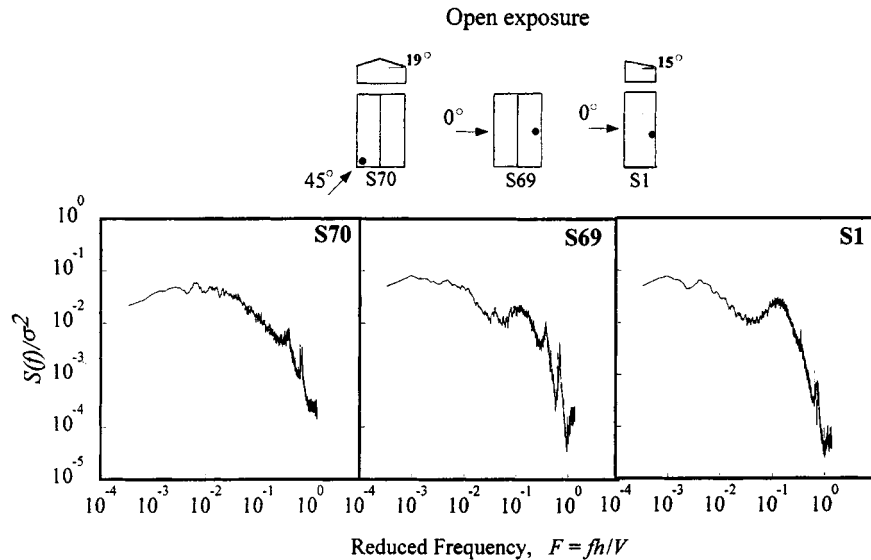Fig. 5 Sample wind pressure spectra on flat roof

Fig. 6 Sample wind pressure spectra on gable and monoslope roofs

both flat (sample S56) and sloped roofs (samples S69 and S1). Similar forms of spectra were also observed by Holmes (1994) and Kasperski *et al.*(1996). Further, Fig. 7 demonstrates the evolution of spectral shapes and the transition from one to the other in the case of a flat roof building in open terrain exposure.

As expected, spectra vary from location to location due to the nature of the physical processes that occur near the roof surface in boundary layer flow. At high frequencies, the amplitudes of spectra seem to be similar; however, they are indeed different at the lower frequency ranges where most of the energy lies. Though some properties of time series such as variance, the number of zero down or up-crossings (N_0T), the number of negative or positive peaks (N_pT), the irregularity factor (ε) and the bandwidth parameter (β) can be
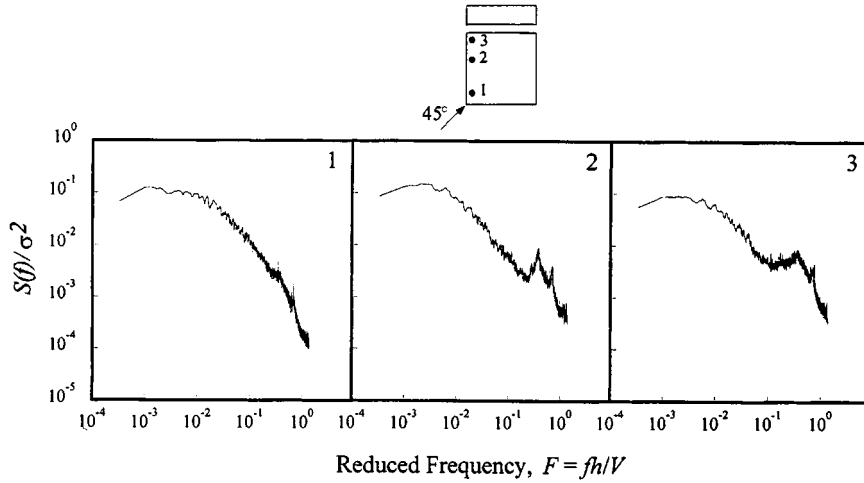
Fig. 7 Evolution of spectral shapes (flat roof)

Table 2 Statistics of the samples

| | Sample | | |
Description	S50	S56	S65
Mean	-0.80	-1.22	-0.87
Variance	0.28	0.13	0.10
Skewness	-2.28	-0.93	-0.35
Kurtosis	9.82	4.69	3.48
N_0T(from signal)	796	1104	1066
N_0T(from spectra)	888	1286	1149
N_pT(from signal)	2001	2039	1900
N_pT(from spectra)	2462	2546	2358
ε	0.36	0.50	0.49
β	0.93	0.86	0.87

deduced from spectra, other properties such as mean, Gaussian or non-Gaussian nature, information about spikes etc. of the corresponding time series cannot be deduced from them. Table 2 shows the statistics of the fluctuations of the sample shown in Fig. 5. By definition, all the three samples are non-Gaussian since they have a non-zero skewness and a kurtosis value higher than three. Sample S50 is highly non-Gaussian (skewness much less than zero and kurtosis much higher than three), while sample S65 is nearly Gaussian (skewness close to zero and kurtosis close to three) but this information cannot be drawn from spectra. Sample properties (N_0T, N_pT, ε, β) estimated from the corresponding spectra as well as from the time series are also shown in Table 2. As expected, the spectra are characterized as broad-banded from the values of ε and β. This observation is common among all roof taps for all geometries tested. Further, it is noted that the number of zero down-crossings (N_0T) as well as negative peaks (N_pT) estimated using spectra are mostly higher than those of the estimated using time series. This is possibly due to the narrowband assumption used in deriving those
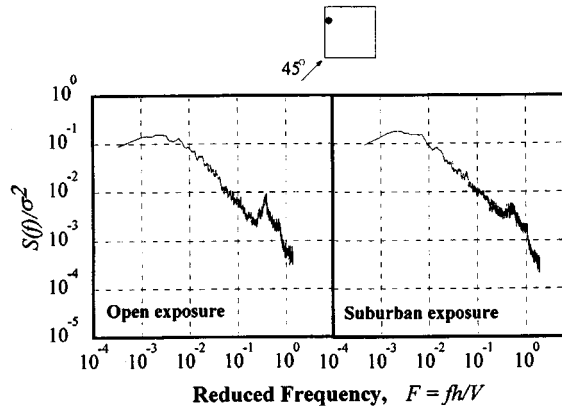
Fig. 8 Comparison of wind pressure spectra at different terrain conditions

estimates.

Fig. 8 compares two spectra measured at the same location on a flat roof in open country and suburban terrain conditions. Even though the variances are different due to the variation in incident turbulence, the normalized spectra appear to be similar. The same characteristics are also found at other locations. Following the inspection of various spectra on the roof, a number of qualitative conclusions can be drawn and summarized as follows :

(a) Though the spectra change in shape and magnitude depending on the geometry of the roof, terrain conditions, wind attack angle and tap location, they can be classified into two categories : (1) spectra whose amplitude decreases as the frequency increases and (2) spectra whose amplitude decreases up to a certain frequency and then grow to have another hump. The growth in the second type of spectra is attributed to the additional contribution from pressure fluctuations in the separation layer.

(b) The variance of fluctuations (area under $S(f)$) is different for different conditions. For comparison purposes, all spectra have been normalized with respect to their variance and many characteristic spectra normalized in this way seem to be similar in shape and magnitude. This is a favourable characteristic for the analytical description of spectral curves.

(c) The normalized pressure spectra corresponding to the same tap in open and suburban terrain conditions are similar, though the variance is greater in case of suburban conditions, as expected.

Since normalized spectra measured at various locations of the roof under different conditions show similarities, there is a possibility to construct an empirical expression to represent spectral curves, as discussed in more detail in the following section. Standard spectral shapes may be proposed for different zones of the roof. The actual pressure spectra at the corresponding location can be obtained by simply multiplying the standard shape by the corresponding variance

5. Representation of spectra

As previously discussed, spectral curves can be represented by empirical equations and thereby Fourier amplitudes can be generated in a synthetic manner. Though spectra of pressure fluctuations at various taps appear generally similar in shape, the spectral amplitudes vary

depending on the variances of the corresponding fluctuations. In order to simplify the empirical modelling as well as to get standard spectral shapes, all spectra have been normalized by their variance. Thereafter, several traditional curve fitting techniques have been employed to extract a suitable empirical equation for spectra. Because of the initial lack of success, a different approach by using trial and error was attempted. A least-square optimization approach has been adopted to fit a spectrum with a given function. The Levenberg-Marquardt algorithm known for its robustness along with cubic polynomial interpolation line search method has been used to carry out least-square optimization(MATLAB 1994).

Several functions representing approximately the same shape as the target spectra have been tried. A SDF's monotonic decay in amplitude with increasing frequency (a straight line decay in logarithmic scale) indicates that a power function of the form $f^{-\alpha}$, where α is the power index and f is the frequency might be suitable but not for low frequencies where most of the energy lies. The hump that is noticed in several spectra cannot be represented by this function. After an extensive investigation, an exponential function has been found to be more appropriate. Moreover, under general conditions, the periodogram ordinates (linearly proportional to the spectrum ordinates) at any set of frequencies are asymptotically independent exponential random variables (Brockwell and Davis 1991) which reinforces the suitability of this function. The proposed function is

$$S(f)/\sigma^2 = a_1 e^{-c_1 f} + a_2 e^{-c_2 f} \tag{8}$$

where, $S(f)$ is the spectral ordinate, σ^2 corresponds to variance, f corresponds to frequency, a_1 & a_2 are the position constants and c_1 & c_2 are the shape constants. The position constants control the location of the spectra, whilst the shape constants control their shape. The proposed function consists of two exponential functions; $a_1 e^{-c_1 f}$ represents the amplitudes in the high frequency range, while $a_2 e^{-c_2 f}$ represents the amplitudes in the low frequency range. The four parameters (a_1, a_2, c_1 and c_2) corresponding to a particular data set can be estimated; initial guesses are made only for c_1 and c_2 since the other two parameters (a_1 and a_2) can be easily found using Eq. (8) written in the matrix form,

$$[S(f)/\sigma^2] = [\overset{(m \times 1)}{e^{-c_1 f}} \overset{(m \times 2)}{e^{-c_2 f}}] [\overset{(2 \times 1)}{a_1 a_2}]^T \tag{9}$$

Then,

$$[a_1 a_2]^T = [e^{-c_1 f} e^{-c_2 f}] \backslash [S(f)/\sigma^2] \tag{10}$$

is the solution in the least-squares sense to the overdetermined system of Eq. (9) computed by Gaussian elimination where, the symbol '\' represents the matrix left division operator (MATLAB 1992). Further, the substitution of Eq. (8) in (7) would result in

$$\frac{a_1 c_2 + a_2 c_1}{c_1 c_2} = 1 \tag{11}$$

By using Eq. (11), one of the spectral parameters can be determined by knowing the other three. Therefore, the SDF can be simulated by knowing any three parameters.

An example of the measured and fitted wind pressure spectra is shown in Fig. 9. The spectral fit appears satisfactory; for instance, the spectral fit has $N_0 T = 931$, $N_p T = 2459$, $\varepsilon = 0.38$ and $\beta = 0.925$ which are close to the corresponding values calculated from target spectra
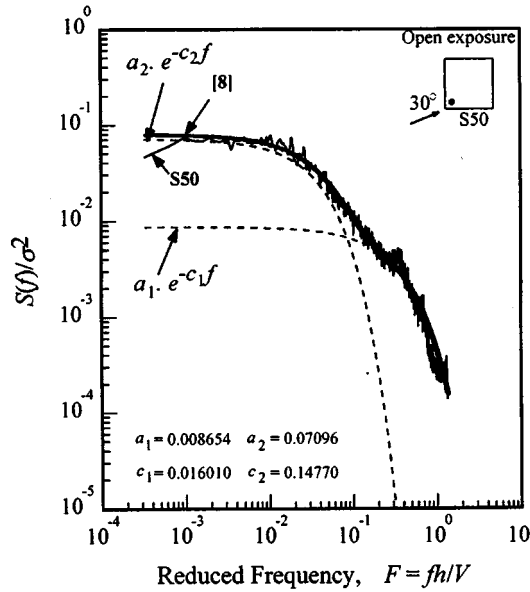
Fig. 9 Measured and fitted wind pressure spectra (flat roof)

provided in Table 2. Satisfactory performance of the proposed empirical expression has also been observed in a variety of other cases. Though the fit is based on minimizing the squared residuals (i.e., square of the difference between the fitted spectral amplitudes and the measured spectral amplitudes), it was decided to quantify the level of accuracy of the fit based on four spectral statistics (N_0T, N_pT, ε and β) with a view to providing a physical meaning to the error caused by the fit. During this investigation, a number of case studies have shown that the above spectral statistics can be obtained within 10% using this fitting procedure which is reasonable for practical applications.

Further, the evolution of the fitted curve is shown in Fig. 9 by plotting $a_1e^{-c_1f}$ and $a_2e^{-c_2f}$ separately. It is clear that the term $a_1e^{-c_1f}$ controls the position and shape of spectra in the higher frequency region, while the term $a_2e^{-c_2f}$ controls the position and shape of spectra in the lower frequency region. The term $a_1e^{-c_1f}$ shifts the ordinate of the spectra on the right side and thereby represents the additional growth noted in some cases. It is interesting to note that the parameters obtained in the above fitting are all positive and therefore, the derivative of Eq. (8) at any point is a negative quantity which reveals that the fitted curve does not have an upward slope. As a result, this fitting can represent only very mild growth in spectra and it needs modification to fit the predominant spectral growth observed in some cases such as samples S69 and S1 shown in Fig. 6. In such cases, spectra show a clear hump and the proposed Eq. (8) requires an additional term $a_3e^{-c_3f}$ to fit the data efficiently; the modified function is

$$S(f)/\sigma^2 = a_1e^{-c_1f} + a_2e^{-c_2f} + a_3e^{-c_3f} \tag{12}$$

The parameters a_3 and c_3 can be established using the previously mentioned fitting procedure with some minor modifications in the program; these include the addition of new term $a_3e^{-c_3f}$ in Eq. (8), the corresponding changes in Eqs. (9) and (10) and the incorporation of c_3 in the list of initial guesses. Fig. 10 demonstrates a typical example of a fit where the spectral
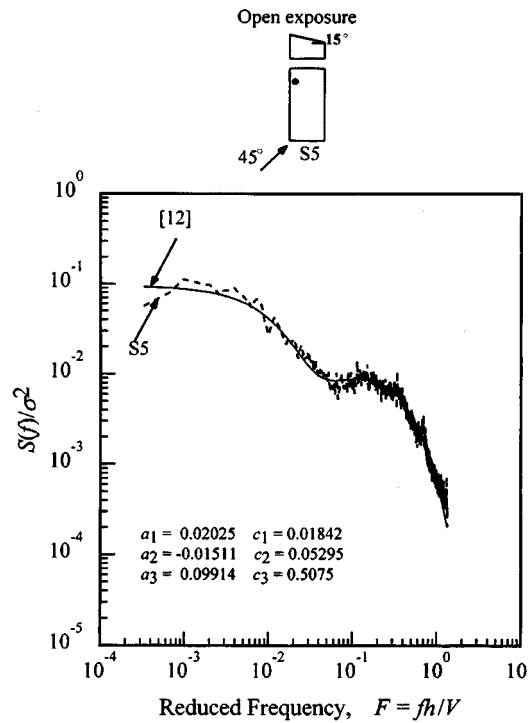
Fig. 10 Measured and fitted wind pressure spectra (monoslope roof)

growth at certain frequencies is predominant. Note the negative value obtained in the case of parameter a_2 by which the upward slope in fitting is established to represent the hump. Finally, it is noted that Eq. (8) can efficiently represent spectra in most of the locations of various roof geometries for different azimuths; however, Eq. (12) is required to represent the predominant spectral growth observed in few cases, to be specified later in this paper.

A typical example illustrating the sensitivity of spectral parameters is shown in Fig. 11, in terms of the variation of spectral statistics with respect to the variation of spectral parameters. The spectral fit shown in Fig. 9 is used for this demonstration. Each time, one of the spectral parameters is varied around its optimum value and the corresponding variations of spectral statistics are plotted. It is clear from Fig. 11 that the spectral statistics are most sensitive to c_1, when varied around its optimum value of 0.01601-see Fig. 9. Note that c_1 determines the dying out rate in the high frequency range representing the energy content in small scale turbulence generated by the building. The spectral statistics are not as sensitive to parameters a_1, a_2 and c_2 in comparison with c_1. In the cases of parameters a_2 and c_1, the spectral statistics such as ε, N_0, and N_p reduce with increasing parameter values, while β increases with increasing parameter values. However, in the cases of parameters a_1 and c_2, the spectral statistics such as ε, N_0, and N_p increase with increasing parameter values, while β reduces with increasing parameter values. Note that as ε increases, β decreases and vice versa which is expected from Eq. (6). Moreover, as ε decreases, N_0 also decreases and vice versa. This is because as ε decreases, the process tends to become broadbanded and consequently, the number of zero up-crossings is expected to be reduced. Similar trends are observed in other spectra.
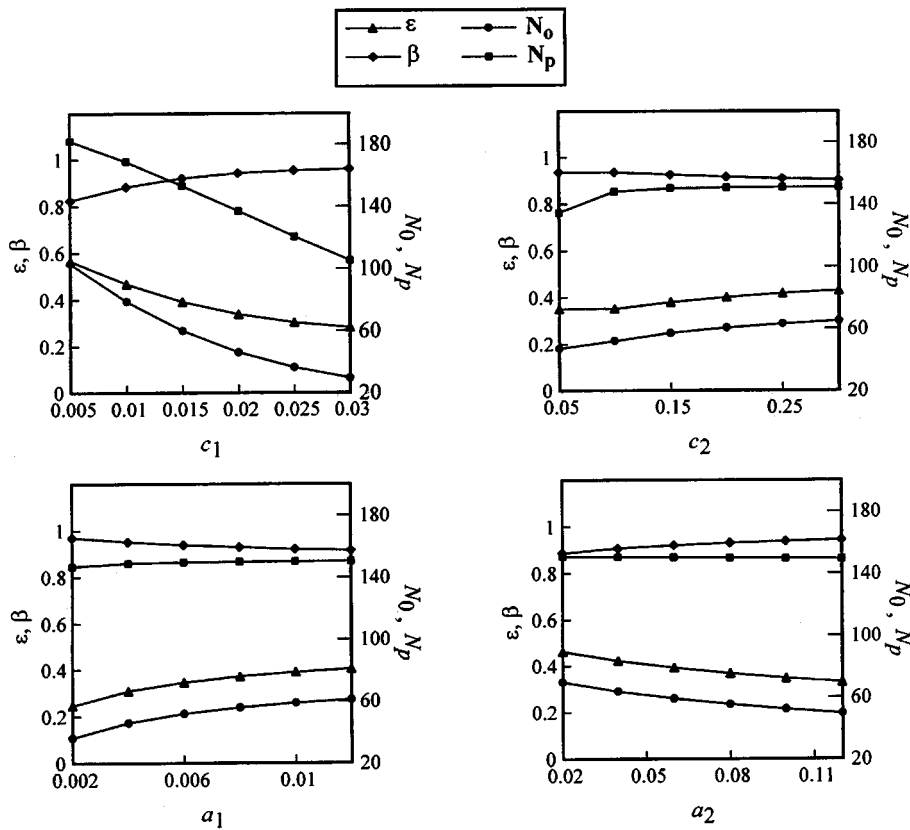
Fig. 11 Sensitivity of spectral parameters (case-Fig. 9)

6. Generalization

As previously discussed, it is possible to group normalized pressure spectra on roofs due to their similarities. Further, it is of practical interest to categorize all types of spectra on roofs into a certain limited number of groups. Since the simulation methodologies used for Gaussian and non-Gaussian time series simulations are different, it would be better to classify the zones of Gaussian and non-Gaussian regions prior to the grouping of spectra in the respective regions. Within this context, the zones of Gaussian and non-Gaussian fluctuations are identified for range of wind direction for each roof based on skewness and kurtosis of pressure fluctuations. Fig. 12 shows the skewness and kurtosis values of the pressure fluctuations measured for various roof configurations. The general trend is that when skewness decreases, there is a quasi-proportionate increase in kurtosis value. Further, pressure fluctuations with low skewness value (say, above -0.5) and high kurtosis value (say, above 3.5), or with high skewness value (say, below -0.5) and low kurtosis value (say, below 3.5) rarely occur. In a few cases, kurtosis values exceeded 3.5 but only up to 4.0 for fluctuations with low skewness values. On the basis of these observations, a particular region is considered non-Gaussian if the absolute values of skewness and kurtosis of pressure fluctuations at various taps are greater than 0.5 and 3.5 respectively. The outcome of this exercise is the approximate Gaussian and non-Gaussian regions of flat, gable and monoslope roofs. Fig. 13 shows the
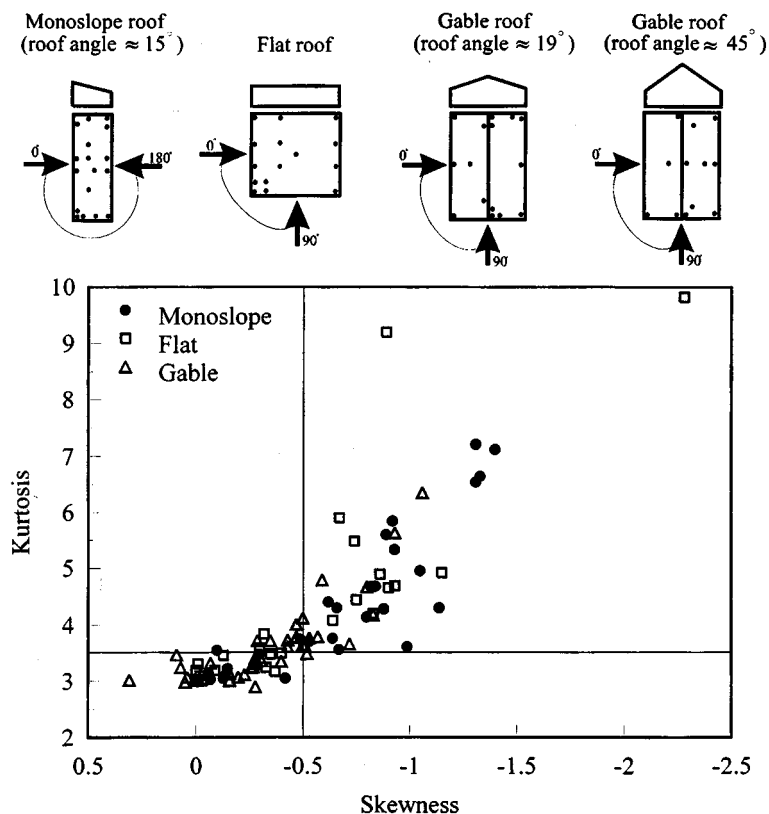
Fig. 12 Skewness and kurtosis values of measured pressure fluctuations

approximate Gaussian and non-Gaussian zones for a 15° monoslope roof; where z is assumed to be 10% of the least horizontal dimension or 40% of lower eave height whichever is less (NBCC 1995).

Generally, the spectra observed in Gaussian regions appear to have more erratic spikes due to their low variance; however, normalized spectra seem to be similar irrespective of location and wind direction. For instance, Fig. 14 shows the normalized spectra measured at different locations on a flat roof in different terrain conditions for zero wind direction. The spectra appear to have more or less similar shapes. This has been noted at several locations of a flat roof for other wind directions. Since their shapes are similar, pressure spectra are averaged to obtain the most probable spectra for that region. Thereafter, the proposed empirical function is fitted as previously discussed. The statistics of the fitted spectra are compared with those corresponding to the observed in Table 3. Note that this fitting is based on twelve measured spectra from this Gaussian region. In most of the fittings, the spectral statistics are obtained within 20% and this discrepancy is due to the averaging of several spectra. In the case of the non-Gaussian region, two types of spectra have been found; the first type observed in windward regions has generally decreasing amplitudes while the second, observed on the farwind and leeward regions has another hump. Based on this, the non-Gaussian region is again divided into two zones. Consequently, spectra have been averaged in corresponding zones and fitted by the empirical expression.

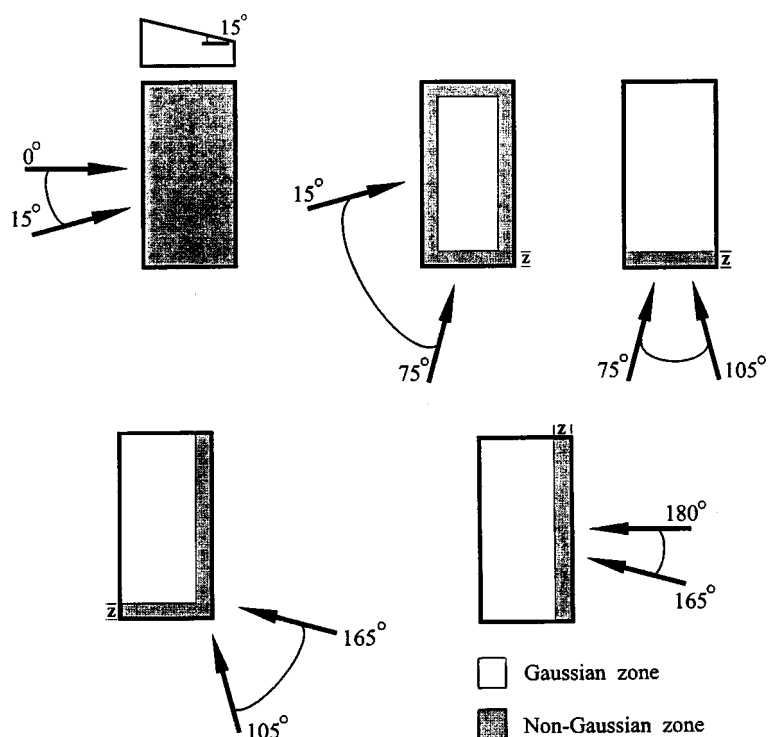This procedure has been carried out for monoslope as well as gable roofs. In the case of

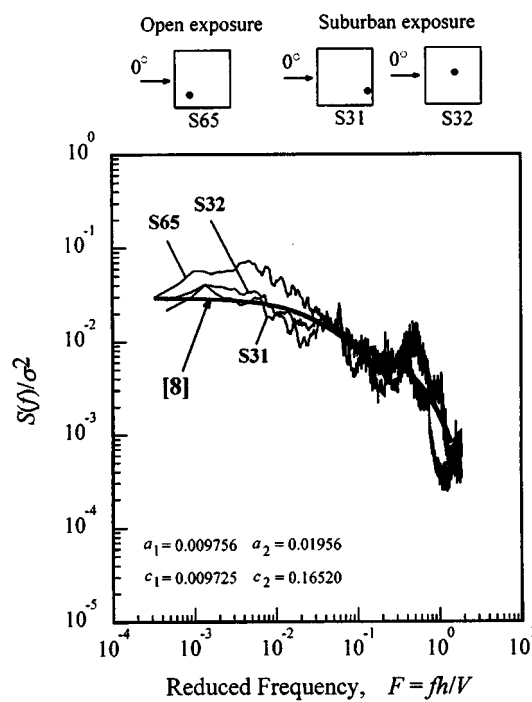Fig. 13 Gaussian and non-Gaussian zones for monoslope roofs

Fig. 14 Measured and fitted wind pressure spectra (flat roof, Gaussian zone)

Table 3 Comparison of spectral properties (flat roof, Gaussian zone)

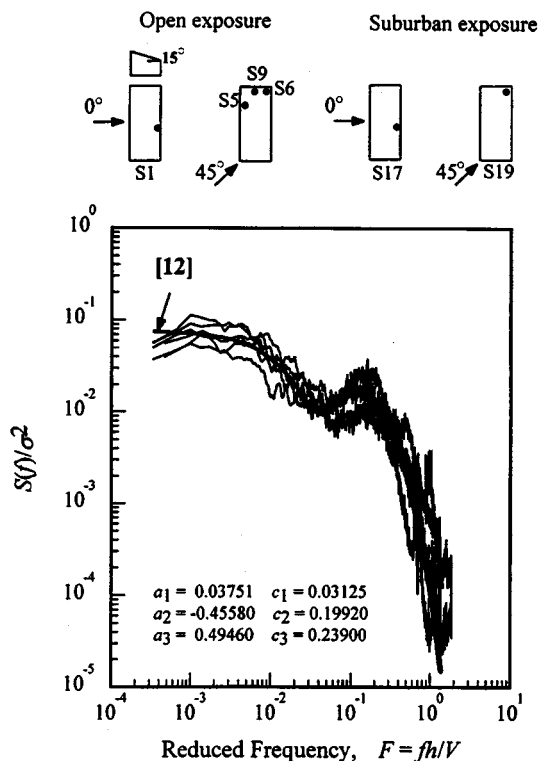| Sample	N_0	N_p	ε	β
Fit	94.9	169.8	0.56	0.83
S65	70.2	143.9	0.49	0.87
S31	88.5	153.5	0.58	0.82
S32	80.1	144.7	0.55	0.83

Fig. 15 Measured and fitted wind pressure spectra (monoslope roof, non-Gaussian zone)

monoslope roofs, two types of spectra in Gaussian zone have been observed; the first type lies in the interior and the other type lies on the edges of the roof. In farwind as well as leeward non-Gaussian regions of the monoslope roof, the spectra seem to indicate a clear hump at high frequencies. In this particular case, the proposed Eq. (12) is required to fit the data efficiently. A typical example provided in Fig. 15 shows several normalized spectra from the corresponding regions of the monoslope roof and the fitted curve. In the case of the gable roof ($\alpha \approx 19°$), the normalized spectra in Gaussian zones are found to be identical with those in Gaussian zones of the flat roof; therefore, the same spectral parameters have been adopted. In the case of the gable roof with roof angle 45°, the normalized spectra from various regions for different wind angles appear similar and therefore, a single representative spectrum is proposed.

The grouping of spectra has been carried out for various roof geometries. The results are summarized in Figs. 16~18, where the standard SDF shapes associated with different regions
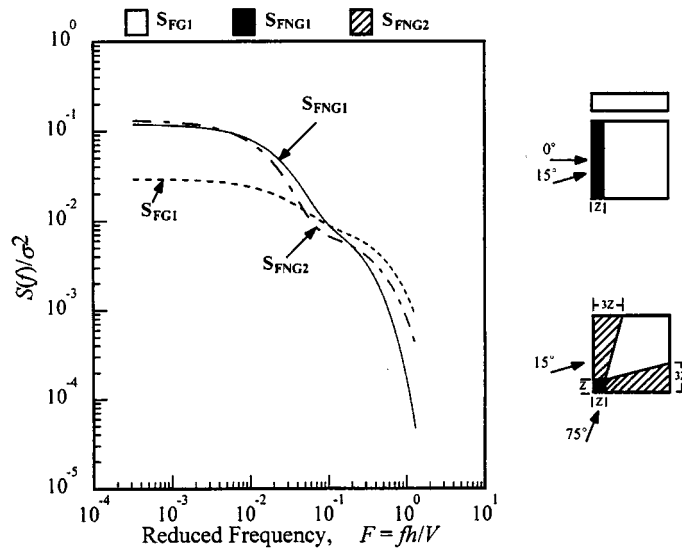
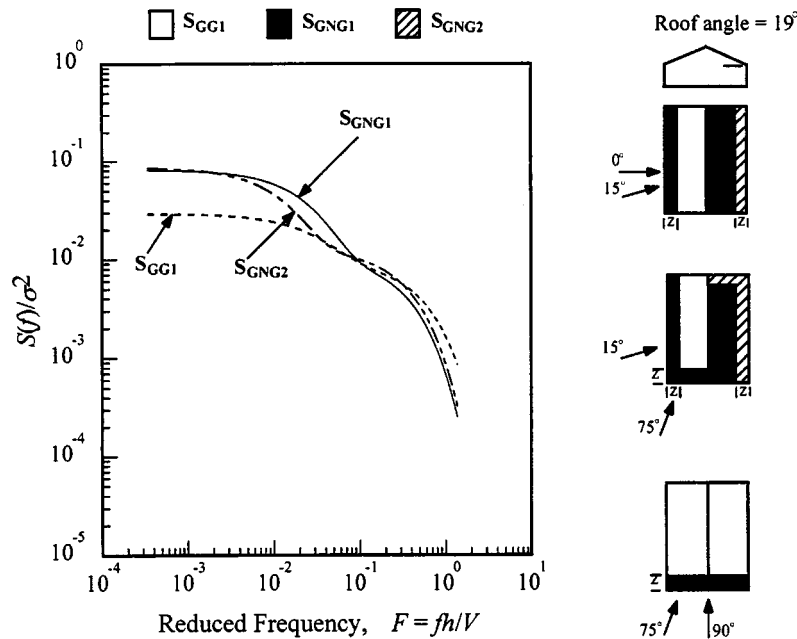Fig. 16 Standard spectral shapes for flat roof

Fig. 17 Standard spectral shapes for gable roof

of the roofs are provided for various roof geometries. Each spectrum is assigned a subscript where the first letter stands for the type of roof, G stands for Gaussian zone, NG stands for non-Gaussian zone and the number stands for the type of spectra in that zone. Since the normalized spectra found in Gaussian regions (S_{FG1}, S_{GG1}, S_{MG1}) are somewhat similar irrespective of the roof geometry, tap location, wind direction and terrain conditions, they have been averaged and fitted by the empirical expression. As a result, Figs. 16~18 show
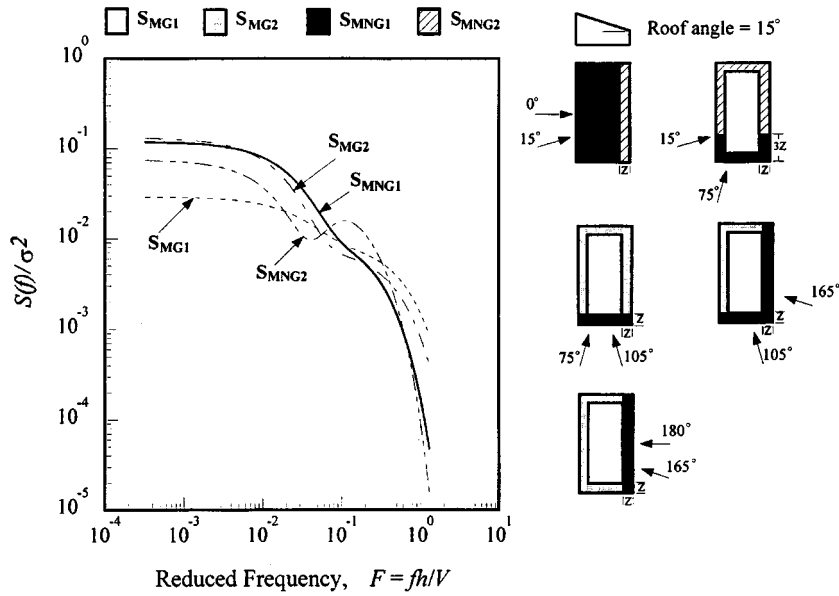
Fig. 18 Standard spectral shapes for monoslope roof

Table 4 Proposed spectral parameters

	a_1	a_2	a_3	c_1	c_2	c_3
			Parameters ($\times 10^{-2}$)			
			Flat Roof			
S_{FG1}	0.9756	1.9560		0.9725	16.5200	
S_{FNG1}	1.2070	11.6100		1.9770	30.1500	
S_{FNG2}	0.8162	12.0500		1.0840	38.2300	
			Gable Roof ($\alpha \approx 19°$)			
S_{GG1}	0.9756	1.9560		0.9725	16.5200	
S_{GNG1}	1.0620	7.1800		1.4990	22.1600	
S_{GNG2}	1.2920	7.4560		1.4730	44.1200	
			Monoslope Roof ($\alpha \approx 15°$)			
S_{MG1}	0.9756	1.9560		0.9725	16.5200	
S_{MG2}	0.8203	12.4900		1.2020	32.9600	
S_{MNG1}	1.2220	10.8000		2.2230	24.0400	
S_{MNG2}	3.7510	-45.5800	49.4600	3.1250	19.9200	23.9000
			Gable Roof ($\alpha \approx 45°$)			
	2.4560	17.6900		4.1050	49.5300	

identical spectra in the corresponding regions. The comparison provided in Figs. 16~18 between the first type of spectra observed in non-Gaussian regions (S_{FNG1}, S_{GNG1}, S_{MNG1}) among the various roof geometries shows that their shapes are somewhat similar. However, there are large variations among SDF shapes in the case of the second type of spectra observed in non-Gaussian regions among the various geometries tested. The data available may not be

sufficient to group the spectra among various geometries; however, the provided SDF shapes can be used to establish actual spectra corresponding to a particular tap for a specific geometry by multiplying the equation of the appropriate SDF shape by the corresponding variance. Parameters of SDF shapes are provided in Table 4. Note that the position constant, a_2, corresponding to spectra from Gaussian regions is lower than that of non-Gaussian regions which reveals that the spectra from non-Gaussian regions are located above spectra from Gaussian regions in the low frequency range. Similarly, the shape constants (c_1 and c_2) corresponding to spectra from Gaussian regions are lower than those of spectra from non-Gaussian regions; this shows that the reduction rate of spectral amplitudes from Gaussian regions is generally lower than that of spectral amplitudes from non-Gaussian regions.

Though the results provided are based on limited measurements, it is believed that a larger database of measurements in the future could improve the proposed zoning as well as the associated spectral parameters, and include spectral parameters for various other geometries.

7. Application

The application of the developed standard SDF shapes is briefly described here. First, from the knowledge of variance of pressure fluctuations at a desired roof location, spectra of pressure fluctuations at the same location can be synthetically generated using standard SDF shapes provided in this study. Thereafter, the simulation scheme proposed by Suresh Kumar (1997) can be utilized to generate Gaussian as well as non-Gaussian pressure fluctuations on roofs. Fourier amplitude as well as phase are required for this simulation. The Fourier amplitude can be easily constructed from synthetic spectra. A simple stochastic model with a single parameter b, inducing non-normality in the time series is suggested for the simulation of phase of non-Gaussian signals. In the case of Gaussian fluctuations, phase is represented by independent identically distributed uniform random numbers ranging between $-\pi$ and π. This model has been applied successfully in the prediction of peaks associated with specified risk levels (Suresh Kumar and Stathopoulos 1997) and in the evaluation of fatigue life estimates (Suresh Kumar and Stathopoulos 1998b).

The measured spectrum (sample S1) and the fit shown in Fig. 15, and the measured spectrum (sample S65) and the fit shown in Fig. 14 were utilized to demonstrate how well the synthetic spectra represent measured spectra in time series simulations. In both cases, the simulations have been carried out using measured spectra (Simulation-I) and using synthetic spectra (Simulation-II) based on the approach described in Suresh Kumar (1997) and Suresh Kumar and Stathopoulos (1997). The results of the simulations I and II are presented in the form of probability density functions in Fig. 19, where the abscissa represents normalized pressure coefficients in the form of (Cp-Cpmean)/Cprms (Cp corresponds to pressure coefficient, Cpmean corresponds to mean pressure coefficient, Cprms corresponds to root-mean-square pressure coefficient). In both cases, the corresponding probability density functions of simulations I & II are close. This observation is further supported by the traditional Chi-Square goodness-of-fit test (Press *et al.* 1989). Similar results prevail in other cases. In addition, Table 5 shows the peak values (maximum suction) of the simulated records. The peak values obtained from Simulation-I and Simulation-II are close in both cases. These results indicate the capability of the proposed empirical model to represent the actual spectra in time series simulations. These are only two cases of the many simulations that have been carried out during this investigation (Suresh Kumar 1997).
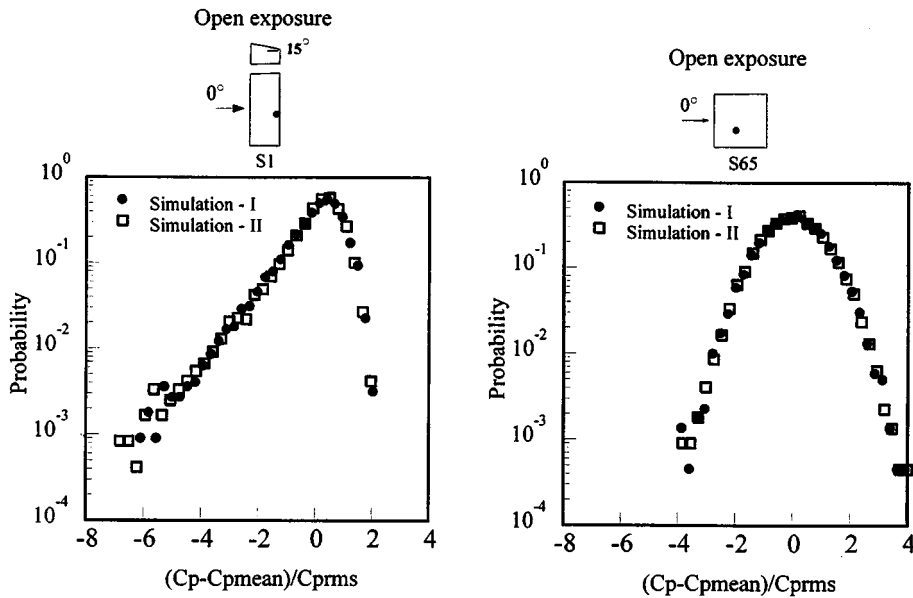
Fig. 19 Probability density functions of simulated signals

Table 5 Comparison of peak values

Sample	Simulation-I	Simulation-II
S1	-3.48	-3.73
S65	-2.15	-2.14

8. Conclusions

An extensive investigation of power spectral density functions of wind-induced pressures acting on low building roofs of different geometries has been carried out. Spectra of wind pressures were found to vary with respect to location, wind direction, roof geometry and terrain conditions. However, similarities between normalized spectra for different conditions have also been observed. On this basis, an empirical form has been suggested for the synthetic generation of normalized spectra. Thereafter, normalized SDF's are classified based on whether the region of interest experience Gaussian or non-Gaussian fluctuations. Finally, the standard spectral shapes associated with various zones of each roof and their parameters have been provided. The application of the developed SDF shapes is also briefly described.

References

Brockwell, P.J. and Davis, R.A. (1991). *Time Series : Theory and Methods*, Springer-Verlag.

Davenport, A.G. (1961), "The spectrum of horizontal gustiness near the ground in high winds", *Quarterly Journal of Royal Meteorological Society*, **87**, 194-211.

Holmes, J.D. (1994), "Wind pressures on tropical housing", *J. Wind Eng. Ind. Aerodyn.*, **53**, 105-123.

Kasperski, M., Koss, H. and Sahlman, J. (1996), "BEATRICE joint project : Wind action on low-rise buildings-Part 1. Basic information and first results", *J. Wind Eng. Ind. Aerodyn.*, **64**, 101-125.

MATLAB. (1992). *High-Performance Numeric Computation and Visualization Software*, The Math

Works Inc., Mass.

MATLAB. (1994). *Optimization ToolBox User's Guide*, The Math Works Inc., Mass.

NBCC. (1995). *User's Guide-NBC 1995, Structural Commentaries (Part 4)*, National Research Council of Canada, Ottawa, Canada.

Panofsky, H.A. and McCormick, R.A. (1954), "Properties of spectra of atmospheric turbulence at 100 metres", *Quarterly Journal of Royal Meteorological Society*, **80**, 546-564.

Press, W.H., Flannery, B.P., Teukolsky, S.A. and Vetterling, W.T. (1989). *Numerical Recipes (FORTRAN)*, Cambridge University Press, Cambridge.

Stathopoulos, T., Surry, D. and Davenport, A.G. (1981), "Effective wind loads on flat roofs", *J. Struct. Eng.*, ASCE, **107**(2), 281-298.

Suresh Kumar, K. (1997), "Simulation of fluctuating wind pressures on low building roofs", *Ph.D. Thesis*, Concordia University, Montreal, Canada.

Suresh Kumar, K. and Stathopoulos, T. (1997), "Computer simulation of fluctuating wind pressures on low building roofs", *J. Wind Eng. Ind. Aerodyn.*, **69-71**, 485-495.

Suresh Kumar, K. and Stathopoulos, T. (1998a), "Power spectra of wind pressures on low building roofs", *J. Wind Eng. Ind. Aerodyn.*, **74-76**, 665-674.

Suresh Kumar, K. and Stathopoulos, T. (1998b), "Fatigue analysis of roof cladding under simulated wind loading", *J. Wind Eng. Ind. Aerodyn.*, in press.

Texas Tech Field Experiment Data Package (1992), Texas Tech University, Lubbock, TX, U.S.A.

Tieleman, H.W. (1995), "Universality of velocity spectra", *J. Wind Eng. Ind. Aerodyn.*, **56**, 55-69.

Vanmarcke, E. (1983). *Random Fields : Analysis and Synthesis*, The MIT Press, Cambridge.

Notations

a_1, a_2, a_3	= position constants
c_1, c_2, c_3	= shape constants
Cp	= pressure coefficient
Cpmean	= mean pressure coefficient
Cprms	= root-mean-square pressure coefficient
F	= reduced frequency
f	= frequency
h	= mean roof height of the building
m_i	= spectral moments
N_0	= zero up-crossing or down-crossing rate
N_0T	= number of zero up-crossing or down-crossing in time T
N_p	= positive or negative peak rate
N_pT	= number of positive or negative peaks in time T
$R(\tau)$	= autocorrelation function
$S(f)$	= spectral density function
T	= time
V	= mean velocity at height Z
V	= mean velocity at mean roof height
Vg	= mean velocity at gradient height Zg
Z	= height
Zg	= gradient height
α	= roof angle
β	= bandwidth parameter
ε	= irregularity factor
σ^2	= variance
τ	= time shift

(Communicated by Chang-Koon Choi)